Article

A Highly Efficient Tribocatalysis of La/ZnO Powders for Degradation of Rhodamine B

Dobrina K. Ivanova [1], Bozhidar I. Stefanov [2] and Nina V. Kaneva [1,*]

[1] Laboratory of Nanoparticle Science and Technology, Department of General and Inorganic Chemistry, Faculty of Chemistry and Pharmacy, University of Sofia, 1164 Sofia, Bulgaria; dobrina.k.ivanova@gmail.com

[2] Department of Chemistry, Faculty of Electronic Engineering and Technologies, Technical University of Sofia, 8 Kliment Ohridski Blvd, 1756 Sofia, Bulgaria; b.stefanov@tu-sofia.bg

[*] Correspondence: nina_k@abv.bg

Abstract: Tribocatalysis is a promising environmental remediation technique that utilizes the triboelectric effect, produced when dissimilar materials interact through friction, to generate charges promoting catalytic reactions. In this work, the tribocatalytic degradation of an organic dye—Rhodamine B (RhB)—has been experimentally realized using pure and 2 mol.% La-modified/ZnO powders, synthesized via a simple hydrothermal method. The effects of annealing on the tribocatalytic activity of the La/ZnO catalysts are also studied at 100 and 500 °C. The La/ZnO-modified catalysts showed an enhanced RhB degradation efficiency with 92% removal within 24 h, compared to only 58% for the pure ZnO. The effects of annealing were found to be detrimental, with RhB removal efficiencies dropping from 92 to 69% in the 100–500 °C range. The catalysts' cycling stability was found to be excellent within three cycles. Ultimately, it is demonstrated that by utilizing La/ZnO powders, contaminated wastewater can be efficiently treated through employing tribocatalysis.

Keywords: tribocatalysis; ZnO powder; lanthanum ions

1. Introduction

The organic pollutants and complex components found in dye wastewater discharged from textile, printing, and other industries are difficult to degrade and are typically present in high concentrations [1,2]. As a result, these pollutants seriously harm the environment, disrupt the ecological balance [3–5], and pose a health risk to humans [6]. Physical adsorption [7], biological techniques [8], and chemical methods [9] have all been used to treat dye wastewater to alleviate these concerns. Nevertheless, these techniques have several drawbacks, including high costs, high energy usage, and secondary pollution. The three catalytic processes—photocatalysis, piezocatalysis, and tribocatalysis—that use energy from the environment (such as solar and mechanical energy) to initiate chemical reactions have steadily emerged as the primary technologies for treating wastewater containing dyes. With its low energy consumption and environmental friendliness, photocatalysis has been used to reduce carbon dioxide [10], produce hydrogen [11], and degrade contaminants in wastewater [12,13].

Nevertheless, photocatalytic systems cannot function in low-light conditions indoors, on cloudy days, or at night because photocatalysis depends on light irradiation at the appropriate intensity and wavelength range. Mechanical energy, such as tidal and hydraulic energy, is far more consistent and continuous than solar energy and can be used as a sufficient complement to photocatalysis. Based on the piezoelectric effect, which is caused by strain-induced built-in polarity that inclines the conduction and valence bands, oxidation and reduction reactions are triggered relative to the piezoelectric catalyst's surface [14,15]. Most of the time, piezocatalyst deformation is achieved through high-frequency ultrasonic energy, which is inapplicable in natural settings. Additionally, it is common for the piezocatalysts to require specific morphologies, such as nanowire and nanosheets,

which are easily deformable and offer a degree of preferential orientation required for the piezoeffect [16–18]. For example, Ning et al. reported a 38% degradation efficiency for ZnO nanoparticles against Methylene blue in 3 h [19]. Jiang et al. reported on the degradation of Methyl orange dye using ZnO@PVDF (1:3, *w/w*) with 52% efficiency in 360 min [20]. A 55% degradation of Rhodamine B within 80 min using ZnO hollow pitchfork structures was presented by Sharma et al. [21]. Porwal et al. reported 78% degradation of Methylene blue in 240 min Bi_2O_3-ZnO-B_2O_3 piezocatalyst [22]. Zhang et al. studied different ZnO contents in the 0–5 wt.% range for the $BiFeO_3$/ZnO heterostructure system and found an increasing trend of 73.4 to 96.9% Rhodamine B removal within 180 min up to 2 wt.% ZnO content, dropping to 55.1% with further increases [23].

Tribocatalysis is a novel catalytic technique that has been developed recently [24–29], which transforms mechanical energy into chemical energy using a small quantity of mechanical energy from the surroundings. It works by rubbing tribocatalysts, which can convert mechanical energy into electrical energy and chemical energy. According to the frictional electrification mechanism, electrostatic charges will be created between the surfaces of two heterogeneous materials when they rub against one another. It is commonly known that the difference in the work function of two materials acts as a catalyst for charge transfer. Other factors that may also influence the amount of triboelectric charge include particle size, surface roughness, and environmental conditions. Depending on its relative polarity, the triboelectric properties can predict whether a material is positively or negatively charged after being rubbed [30].

Tribocatalysis makes it simple to use the abundant mechanical energy present in the environment because the process requires a small amount of it. Additionally, a wide variety of tribocatalysts are available because contact electrification is frequently observed in various materials. Since its initial application to dye degradation in 2019 [24], tribocatalytic degradation has garnered substantial research attention. Tribocatalysts like ZnO [31], CdS [32], $NiCo_2O_4$ [33], and $Bi_{12}TiO_{20}$ [34] have been used in numerous studies examining the tribocatalytic degradation of organic pollutants.

In this study, we employed hydrothermal ZnO and La/ZnO powders as tribocatalysts and examined their properties while stirring. The effects of lanthanum ions, annealing temperatures, and recycling of modified samples are estimated factors influencing tribocatalysis in the breakdown of Rhodamine B. This study offers fresh perspectives on the tribocatalysis of ZnO semiconductors, enhancing ZnO's activity for catalytic degradation through modification with La^{3+} oxide to remove organic pollutants from wastewater.

2. Results and Discussion

2.1. Catalyst Properties

The morphology and microstructure of the samples synthesized at various temperatures (between 100 and 500 °C) were examined in detail using scanning electron microscopy (SEM). The resulting micrographs are displayed in Figure 1. According to the images, there are no morphological differences between the pure and La-modified ZnO products.

Energy-dispersive X-ray spectroscopy (EDS) was used to determine the elements Zn, O, and La present in the modified ZnO powders and were estimated as zinc (54.28 wt.%), oxygen (42.45 wt.%), and lanthanum (3.27 wt.%).

The surface area of the ZnO and La-modified ZnO powders was estimated via Brunauer–Emmett–Teller (BET) analysis, with the representative BET adsorption isotherms shown in Figure 2. The La-modified powder has a higher BET surface area (32.34 m^2/g) compared to the ZnO sample (10.30 m^2/g), annealed at 100 °C, which may suggest that the former case will have an increased expected tribocatalytic activity. The tribocatalytic experiments for Rhodamine B's breakdown demonstrate the impact of this parameter.
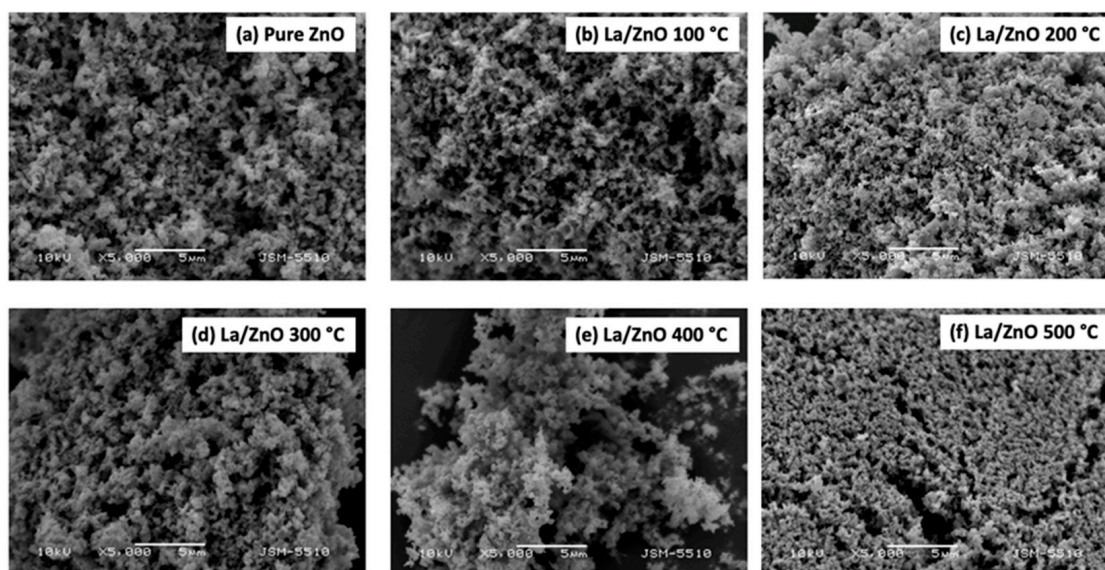
Figure 1. SEM images of powders annealed at different temperatures: (**a**) ZnO, 100 °C; (**b**) La/ZnO, 100 °C; (**c**) La/ZnO, 200 °C; (**d**) La/ZnO, 300 °C; (**e**) La/ZnO, 400 °C; and (**f**) La/ZnO, 500 °C.
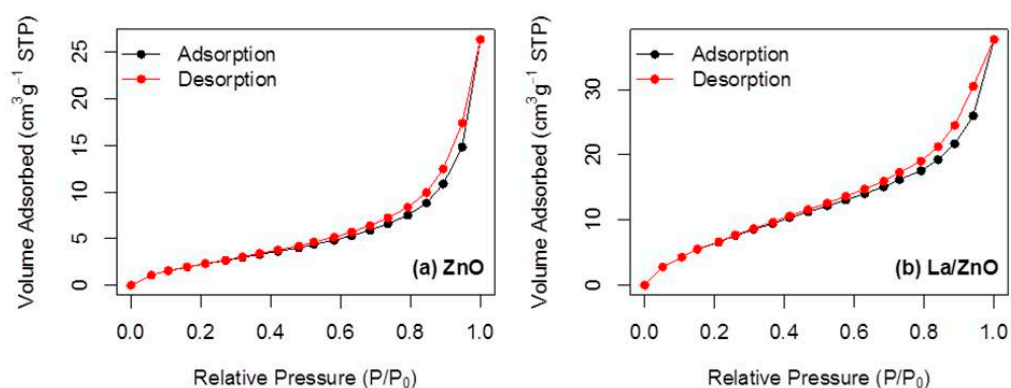

Figure 2. BET adsorption isotherm data obtained for: (**a**) pure ZnO, (**b**) La/ZnO, 100 °C.

The XRD patterns of the ZnO and La/ZnO after annealing at 100 °C, 300 °C, and 500 °C are shown in Figure 3. Every diffraction peak is consistent with PDF #96-230-0117, the standard card, and indicates that the zinc oxide phase is hexagonal wurtzite [35]. The lack of impurity diffraction peaks indicates the high purity of the samples. Strong, sharp peaks in the XRD patterns of the pure and La/ZnO samples indicate a high degree of crystallinity. The XRD patterns of ZnO catalysts modified with La are almost identical to the pure ZnO, suggesting no change in the crystal structure [36], which may indicate that the La_2O_3 phase is evenly dispersed throughout ZnO nanoparticles as small, surface-bound oxide clusters. Additionally, its absence as a distinct phase observable in the XRD patterns of the modified ZnO composites could be attributed to the low concentration (2 mol %). The possibility of surface-bound La_2O_3 is confirmed via Rietveld refinement of the XRD data, employing PowderCell software version 2.3 and a standard wurtzite ZnO datafile, with the resulting data listed in Table 1. The results show that no changes are made to the crystalline lattice parameters; however, a marked effect of the annealing temperature on the average crystallite size is observed.
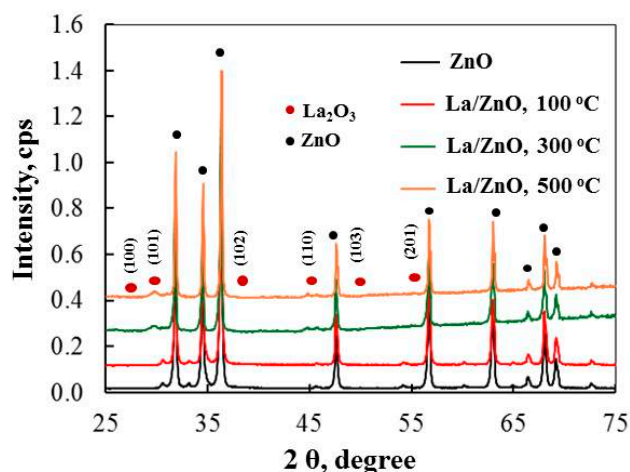
Figure 3. XRD pattern of ZnO and La/ZnO powders annealed at 100, 300 and 500 °C.

Table 1. Crystallite size and parameters of the crystalline lattice of pure and La-modified ZnO powders.

Sample Powders	Crystallite Size, nm	Parameters of the Crystalline Lattice, Å	Microstrains, a.u.
ZnO	36.9	a, b: 3.250 c: 5.207	8.27×10^{-4}
La/ZnO, 100 °C	42.3	a, b: 3.249 c: 5.205	8.32×10^{-4}
La/ZnO, 300 °C	63.9	a, b: 3.248 c: 5.204	1.87×10^{-4}
La/ZnO, 500 °C	78.0	a, b: 3.248 c: 5.204	3.58×10^{-4}

The average crystallite size was obtained via the Debye–Scherrer equation (Equation (1)).

$$D_{hkl} = \frac{0.9\,\lambda}{\beta \times cos\theta} \tag{1}$$

where D_{hkl} is the average crystallite size (nm), λ is the X-ray wavelength of CuKα radiation (λ = 0.154056 nm), β is the full width at half maxima and θ is the Bragg diffraction angle.

To confirm that the La_2O_3 phase is located on the surface of ZnO, transmission electron microscopy (TEM) images of La/ZnO powder, annealed for one hour at 100 °C (later shown to exhibit the best tribocatalytic characteristics), are presented in Figure 4. The figure displays the well-defined ZnO particles and the resulting surface decoration with La_2O_3. These results demonstrate the homogeneous distribution of lanthanum on the zinc oxide particles and the interface formed between them. This finding is in line with other literature examples of lanthanide-modified ZnO catalysts, which consistently show that due to the large difference in ionic radius, in-lattice substitution of Zn with the dopant under mild conditions is unlikely and usually results in a surface-formed separate phase [37,38].
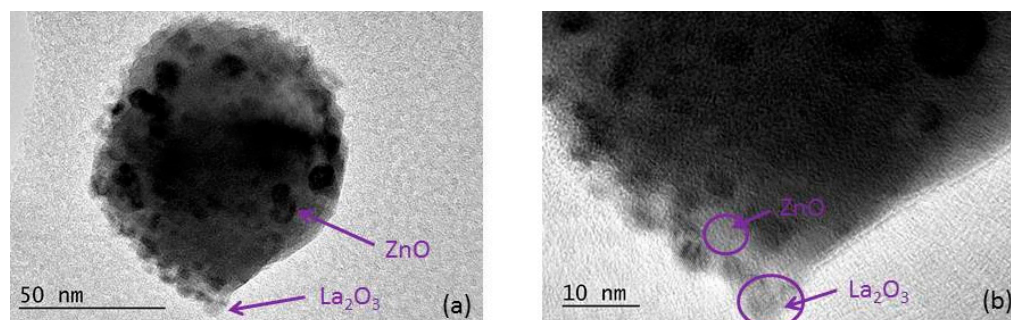
Figure 4. TEM micrographs from selected areas of samples La/ZnO powders annealed at 100 °C at: (**a**) low and (**b**) high magnification.

2.2. Tribocatalytic Efficiency of ZnO and La/ZnO Powders

The tribocatalytic efficiency of ZnO and La/ZnO powders is estimated by tribocatalytic decomposition of Rhodamine B dye in darkness under the action of a magnetic stirrer with a PTFE magnetic bar at 500 rpm. The dye concentrations in all friction tests are the same (10 mg/L). The RhB molecule exhibits a characteristic absorbance at a wavelength of 546 nm, which was used to determine the concentration of the dye solution.

In the absence of the catalyst, there was only a very slight decrease in the 546 nm absorption peak when the magnetic bar was rotated at 500 rpm, as presented in Figure 4. This result showed that the friction between the magnetic bar and glass beaker had little effect on the tribocatalytic process. The effective Rhodamine B degradation was observed only in the presence of ZnO and La/ZnO tribocatalysts, where, within 24 h of magnetic stirring, the distinctive RhB peak gradually diminished, indicating that the dye had degraded.

The tribodecomposition of RhB solution using pure and La-modified ZnO powders annealed at 100 °C is shown in Figure 5a. The results of the degradation process demonstrated that the dye is broken down under the tribocatalytic action. After 24 h of friction, 91.69% of the Rhodamine B is decomposed by the La/ZnO powder.
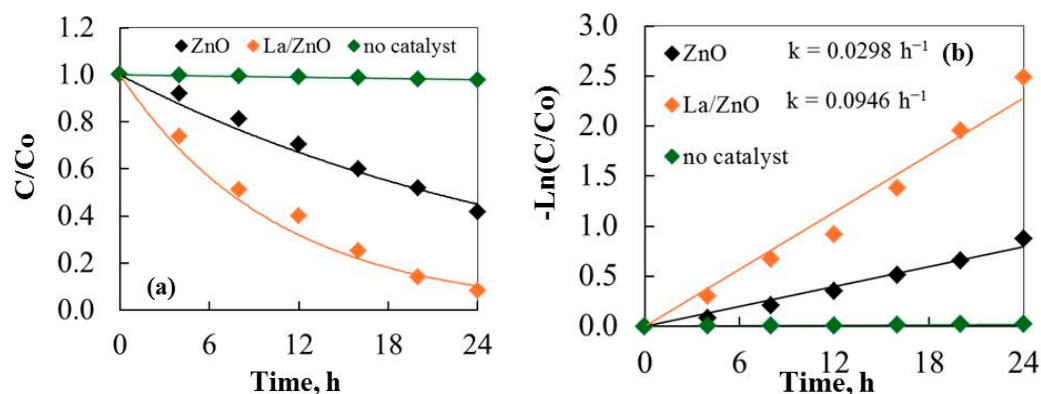

Figure 5. (**a**) Stirring degradation of Rhodamine B solution using ZnO and La/ZnO powders annealed at 100 °C by magnetic stirring conditions, 500 rpm; (**b**) kinetic fitting.

Compared to pure ZnO, the catalytic efficiencies of La/ZnO powders are superior. The results show that specific surface area has a major impact on tribocatalysis. The BET assay expectations are thus confirmed by the tribocatalysis data. The rate constant values (Figure 5b) are determined from the $\ln(C_t/C_0) = -kt$ pseudo-first order approximation and match the trend. The La/ZnO sample exhibits a higher reaction rate ($k = 0.0946$ h^{-1}) compared to the ZnO sample ($k = 0.0298$ h^{-1}). Better tribocatalysis efficiency possibly results from the separation of tribo-generated charge pairs and increased carrier participation in the redox reaction, both facilitated by the higher specific surface area, which has more active sites to participate in and allows more dye to be adsorbed in the reaction [34].

Electrons represent excited e^- and holes represent the formed h^+ that results from ZnO absorbing mechanical energy during friction. During the decomposition of the dye, oxygen molecules react with the electrons, forming superoxide radicals—$O_2^{\bullet-}$. The holes interact with OH^- and are then transformed into hydroxyl radicals—$OH^\bullet$. These radicals attack the RhB molecule, leading to its degradation.

The effective electron–hole separation across the ZnO/La_2O_3 interface and greater production of $O_2^{\bullet-}$ and $OH^\bullet$ radicals could account for the enhanced activity of the La-modified ZnO sample. The higher efficiency can be attributed to an increased number of oxygen vacancies in the La-modified ZnO, caused by the differing charge and electronegativity of lanthanum and zinc ions, as well as the stronger hydroxyl ion adsorption onto the ZnO surface [39,40]. The reaction between the holes and OH^- aids in the creation of $OH^\bullet$. Hydroxide radicals and other tribogenerated active spaces are potent non-selective oxidants that cause degradation of the organic pollutants on the surface of La-modified ZnO [41,42].

The modification of ZnO with lanthanum oxide phase results in the formation of specific energy levels, leading to increased catalytic efficiency, possibly due to the suppression of the tribogenerated charge recombination. Thus, the lanthanum phase is beneficial to incorporate in order to trap electrons, stop electron–hole recombination reactions, and increase the amount of hydroxyl and superoxide radicals, thereby increasing the rate of pollutant degradation.

Evidence for the contribution of hydroxyl and superoxide radicals is provided via a radical scavenger assay that we performed. The data are presented in Figure 6. The contribution of superoxide ($O_2^{\bullet-}$) and hydroxyl ($OH^\bullet$) radicals in the Rhodamine B dye degradation process was quantified by adding ascorbic acid (AA) and isopropyl alcohol (IPA) scavengers, which capture the respective reactive species [40,42].
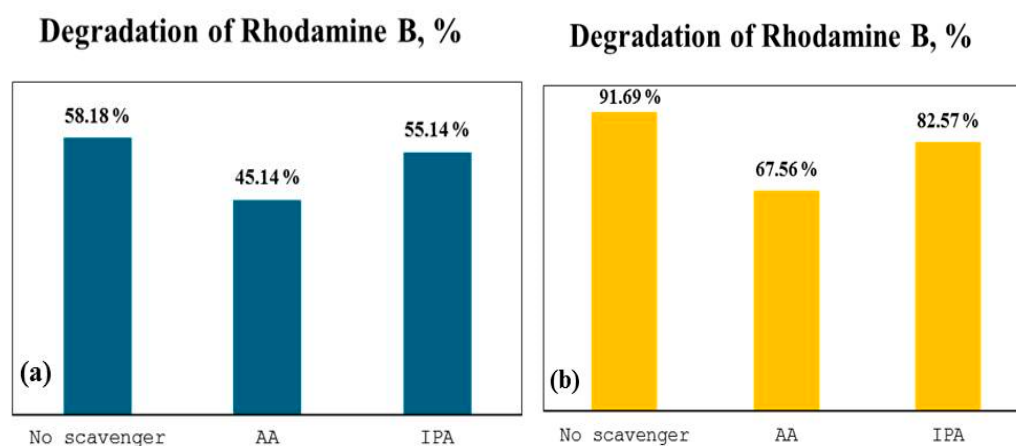

Figure 6. Effect of scavengers on Rhodamine B degradation in tribocatalysis process using (**a**) pure and (**b**) lanthanum-modified ZnO powder.

Figure 6 illustrates that the addition of AA and IPA had a similar effect on both tribocatalyst systems, where a more pronounced inhibition is observed in the former case, thus suggesting that the superoxide radical has a higher influence on the RhB tribodegradation rate.

2.3. Tribocatalytic Efficiency of La/ZnO Powders Annealed at Different Temperatures

The tribocatalytic properties of a series of powders containing 2 mol% of lanthanum phase prepared at 100, 200, 300, 400, and 500 °C are shown in Figure 7a. The figure illustrates how the efficiency of all catalysts decreases as the annealing temperatures rise.
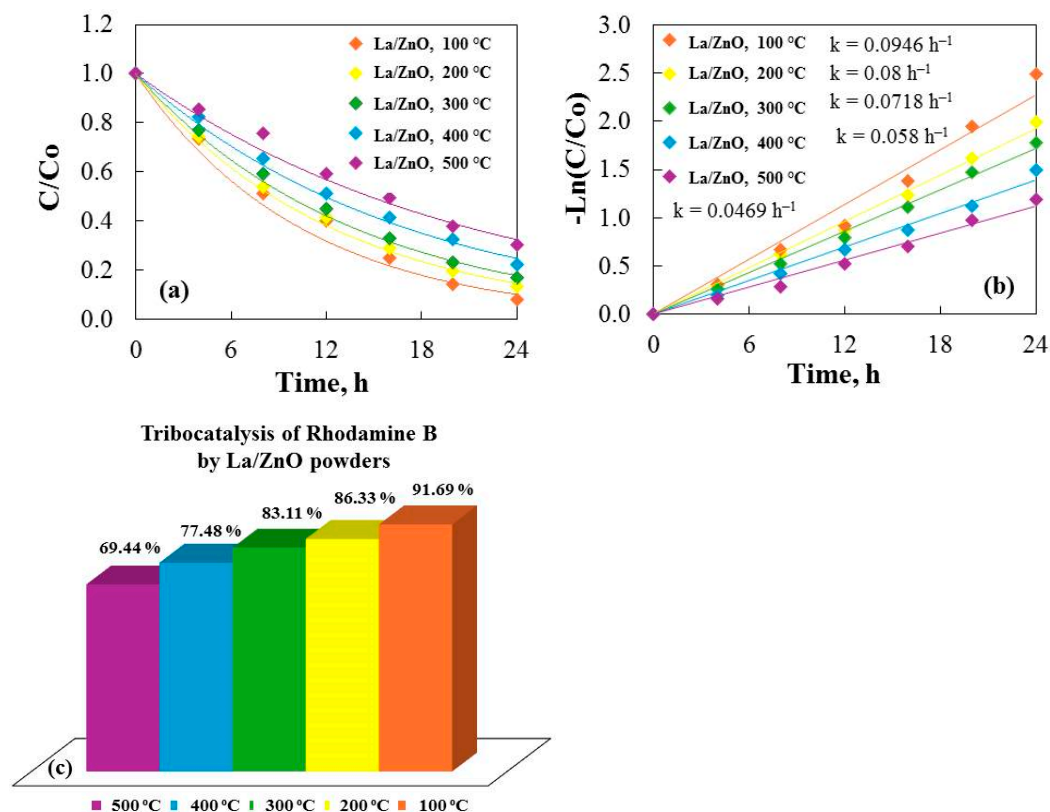
Figure 7. (**a**) Tribocatalytic decomposition of Rhodamine B by La/ZnO powders annealed at different annealed temperatures; (**b**) kinetic fitting; (**c**) degrees of RhB dye degradation versus preparation temperature of La-modified ZnO samples.

The corresponding rate constant values (Figure 7b) support the trend of increased tribocatalytic efficiency at lower preparation temperatures. The modified catalyst annealed at 100 °C yielded the highest reaction rate: $k_{100\,°C} = 0.0946$ h^{-1}, $k_{200\,°C} = 0.08$ h^{-1}, $k_{300\,°C} = 0.0718$ h^{-1}, $k_{400\,°C} = 0.058$ h^{-1}, and $k_{500\,°C} = 0.0469$ h^{-1}. Aggregation of the nanostructures at higher annealing temperatures, resulting from sintering and crystal growth, leads to recombination losses and reduced active surface area, which may cause a decrease in tribocatalytic activity for the catalyst treated at higher temperatures.

Figure 7c confirms and compares the tribocatalytic properties of La/ZnO powders with respect to the degradation of RhB dissolved in distilled water. The decomposition of dye with La/ZnO annealed at 100 °C is 91.69%, while it decreases to 86.33%, 83.11%, 77.48% and 69.44% at 200, 300, 400, and 500 °C, respectively.

To gain further insights into the apparent differences in activity between the pure ZnO and La/ZnO tribocatalysts annealed at different temperatures, attenuated total reflection Fourier transform infrared (ATR-FTIR) spectroscopy measurements were conducted. Figure 8 presents the fingerprint region (900–2000 cm^{-1}) of ATR-FTIR spectra, taken from powder samples aliquoted at the beginning, 12th, and 24th hour of the tribocatalytic Rhodamine B tribodegradation experiments.

In the case of the pure ZnO tribocatalyst (Figure 8a), the only spectral features observed are a broad doublet peaking at 1210 and 1150 cm^{-1}, which becomes more intense throughout the experiment. These bands can be associated with aromatic C-H bending and stretching modes and their appearance has been observed in other studies on the adsorption and degradation of Rhodamine B via heterogeneous photocatalysis [43]. Given that, in the pure ZnO case, they gain intensity as a function of the tribocatalytic process duration, it may be assumed that they are caused by tightly binding intermediates accumulating on the ZnO surface, which may explain the poor activity of the pristine ZnO tribocatalyst.
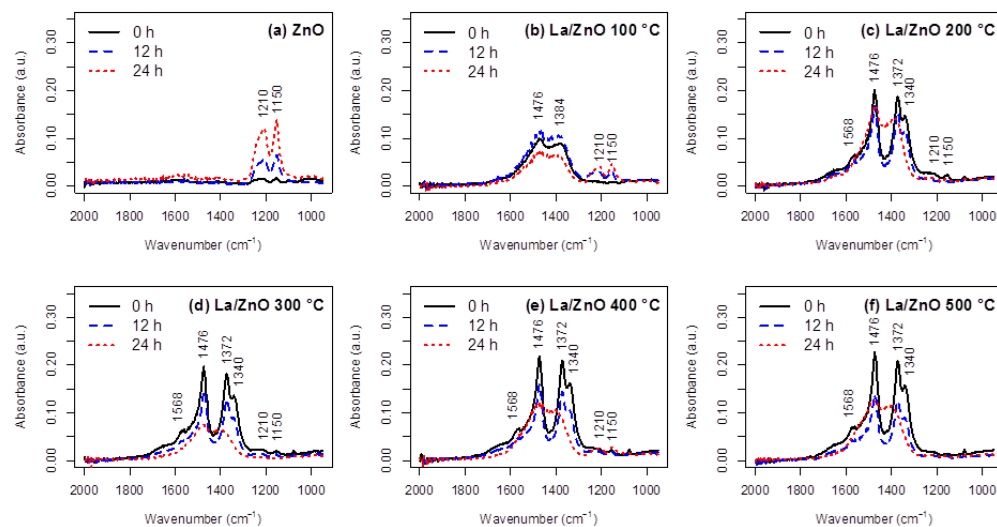
Figure 8. ATR-FTIR spectra obtained for the 0th, 12th and 24th hour of Rhodamine B tribodegradation for: (**a**) pure ZnO; (**b**) La/ZnO 100 °C; (**c**) La/ZnO 200 °C; (**d**) La/ZnO 300 °C; (**e**) La/ZnO 400 °C; (**f**) La/ZnO 500 °C.

A drastic difference is observed in the ATR-FTIR spectra obtained for the La/ZnO tribocatalysts (Figure 8b–f), where, in all cases, regardless of the annealing temperature, two observations can be made: (i) notable features appearing in the 1300–1600 cm^{-1} spectral region; and (ii) the formation of the 1210 and 1150 cm^{-1} peaks is almost completely suppressed. These observations suggest both a stronger molecular bonding of the RhB dye with the La_2O_3 phase and more efficient removal of the RhB intermediates, preventing their accumulation on the La/ZnO surface. For the La/ZnO case annealed at 100 °C (Figure 8b), a poorly resolved doublet is observed with peaks at 1384 cm^{-1} and 1476 cm^{-1}, which lose intensity at the end of the 24 h tribocatalytic run. Increasing the annealing temperature from 200 °C (Figure 8c) to 500 °C (Figure 8d–f) improves the definition of this spectral feature and makes the contributions at 1340 cm^{-1}, 1372 cm^{-1}, 1476 cm^{-1}, and 1568 cm^{-1} more distinguishable, which can be associated with the C–N stretching and C=C modes of the RhB molecule [44]. This suggests that annealing at higher temperatures possibly leads to the recrystallization of the La_2O_3 phase and the formation of structurally uniform RhB adsorption sites, which could explain the improved definition of the FTIR spectra in the tribocatalyst annealed at 500 °C. In all cases, the RhB peaks in the 1300–1600 cm^{-1} range not only lose intensity but also become broader up to the 24th hour, suggesting that the degradation of the RhB molecule actively takes place on the La_2O_3 surface. This aligns with our initial expectation that the La phase in the La/ZnO tribocatalyst provides tribogenerated charge accumulation centers, which are associated with the improved tribocatalytic efficiency.

2.4. Tribocatalytic Effect of Recycle Times of La/ZnO Powders

Tribocatalysis is an environmentally friendly technology that typically poses minimal ecological concerns. Therefore, it is crucial to maintain high efficiency throughout each usage cycle. In this study, we evaluated the stability of the magnetic stirring degradation of RhB by the La/ZnO powders annealed at various temperatures, across multiple cycles. Each cycle involved magnetically agitating 50 mL of RhB solution (10 mg/L) containing 50 mg of La/ZnO sample at a speed of 500 rpm. Following the tribocatalysis process, the powders and RhB were centrifuged, and the La/ZnO sample was dried, rinsed multiple times with distilled water, and then used in subsequent cycles.

Figure 9 shows the results of a study on the regeneration and reuse of hydrothermal powders of La/ZnO. With each cycle, it is clear that the powders' catalytic qualities progressively declined. For each of the five types of catalysts in distilled water, the tribocatalytic

degradation of the dye dropped by about 2% after three cycles. However, throughout these cycles, the dye's tribocatalytic degradation rate remained within an acceptable margin, indicating that the La/ZnO powders exhibited good cycling stability for RhB degradation. The findings confirmed the high degree of tribocatalytic activity of La/ZnO (100 °C) nanostructures even after three cycles of experiments.
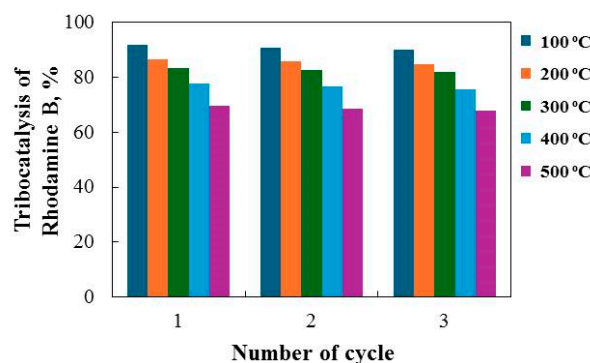

Figure 9. Tribocatalytic degradation rate of Rhodamine B for three consecutive cycles using La/ZnO powders, annealed at different temperatures.

2.5. The Reaction Pathway for the Degradation of Rhodamine

A plausible degradation pathway of Rhodamine B, induced by a reaction with radicals, has been reported in the literature [45]. Initially, the RhB molecule undergoes de-ethylation in response to oxidizing h$^+$ and the related OH$^•$ radicals, producing intermediate compounds such as C1–C6 (viz. Figure 10). Subsequently, the conjugated structure of these de-ethylated products is continuously broken down, forming phthalic acid, resorcinol, and 2,5-dihydroxybenzoic acid.
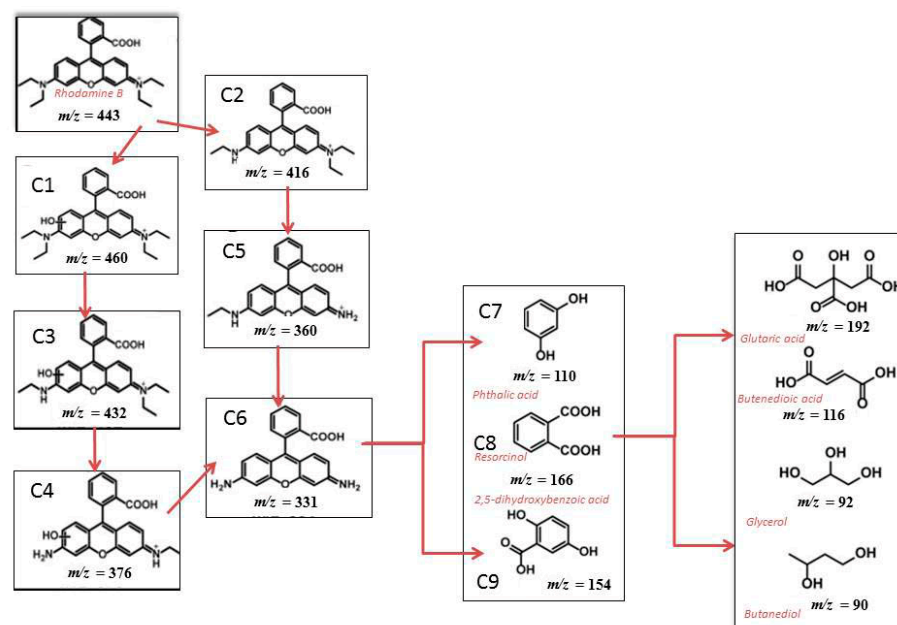

Figure 10. Plausible tribocatalytic degradation pathway of Rhodamine B. Mechanism adapted with permission from Ref. [45].

Further degradation of the benzene ring in C7–C9 (viz. Figure 10) results in the formation of small-molecule organic acids, such as glutaric acid, butenedioic acid, glycerol, and butanediol, devoid of benzene rings. Ultimately, these small organic molecules decompose into water and carbon dioxide.

3. Materials and Methods

The primary substances utilized in this study were Rhodamine B (RhB; $C_{28}H_{31}ClN_2O_3$, $\lambda_{max} = 546$ nm), zinc oxide commercial powder (ZnO, >99.0%), lanthanum (III) oxide (La_2O_3, >99.0%), and absolute ethanol (C_2H_5OH, >98.0%), all of which were obtained from Fluka, Buchs, Switzerland. Distilled water was used in all experiments.

La/ZnO composite powders were produced via a simple and ecologically friendly hydrothermal process. La-modified tribocatalysts were prepared by mixing commercial ZnO powder with La_2O_3 (2 mol%) in a glass vessel, using ethanol as a solvent. The La/ZnO powders required for tribocatalytic testing were created by stirring the materials for ten minutes, sonicating them for thirty more minutes, and then annealing them for an hour at 100 °C. To examine the impact of preparation temperature on the tribocatalytic activity, the remaining La/ZnO materials were annealed for one hour at different temperatures: 200, 300, 400, and 500 °C.

X-ray diffraction (XRD) patterns of the catalysts were obtained on a Siemens D500 diffractometer (CuKα radiation within 2θ range 25–75° at 2θ step of 0.05° and integration time of 2 s/step, Karlsruhe, Germany). The average crystallite sizes were estimated accord-ing to Scherrer's equation and via Rietveld analysis with the PowderCell 2.3 software package and a standard ZnO datafile. Scanning electron microscopy (SEM, Hitachi TM4000, Krefeld, Germany, 10 kV acceleration voltage) equipped with an energy dispersive X-ray spectrometer (EDS, EDXdetector: Quantax 200, Bruker Resolution 126 eV, Berlin, Germany) was used to explore the morphology and element distribution of tribocatalysts. Transmission electron microscopy was performed on a JEOL JEM-2100 (JEOL Ltd., Tokyo, Japan), operating at 200 kV. Based on Brunauer–Emmett–Teller (BET) N_2 absorption (Quantachrome Instruments NOVA 1200e, Boyton Beach, FL, USA), the surface area of pure and RE/ZnO composite powders was estimated. The samples underwent a four-hour degassing process at 150 °C before the N_2 adsorption.

Tribocatalysis was used for the decomposition of RhB (50 mL) solution. The dye was prepared with distilled water in a 100 mL glass beaker, equipped with a magnetic stirrer. In the absence of light, the tribocatalytic reaction was carried out under constant room temperature conditions (23 ± 2 °C). Rhodamine B was initially present at a concentration of 10 ppm. A glass reactor holding dye solution was filled with 50 mg of catalyst (pure or La^{3+}-modified ZnO). The suspension was then magnetically stirred using a magnetic bar that was sealed with polytetrafluoroethylene (PTFE). The resultant mixture was magnetically stirred with a PTFE for 30 min in the dark to achieve adsorption equilibrium between the Rhodamine B solution and tribocatalysts. Subsequently, the reactor is triggered, spinning at 500 revolutions per minute at first. Two-milliliter aliquot samples of the reaction solution were taken regularly. Then, at 6000 rpm, the tribocatalyst was centrifuged. The UV–vis spectra of RhB were obtained using an Evolution 300 Thermo Scientific spectrophotometer (Madison, WI, USA) in the 300–700 nm range.

Additional information about the tribodegradation of the Rhodamine B dye was obtained via attenuated total reflection Fourier transform infrared (ATR-FTIR) spectroscopy. FTIR spectra were obtained on the powdered samples employing a Cary 630 spectrometer, equipped with a Diamond ATR accessory (Agilent Technologies, Inc., Santa Clara, CA, USA).

Furthermore, blank experiments without stirring were performed—there was no sign of any direct degradation of the dye.

A scavenger test was used to look into the reactive species that were causing the Rhodamine B dye to degrade. As scavengers, isopropyl alcohol (IPA) and ascorbic acid (AA) were employed to capture hydroxyl and superoxide radicals, respectively. Then, 6 mM of each scavenger was added in separate runs to pinpoint the precise reactive species that underwent tribocatalysis-induced degradation of the organic dye (50 mL).

4. Conclusions

The La/ZnO samples annealed at 100 °C exhibited the highest degradation efficiency among the five La/ZnO powders tested at various annealing temperatures. These samples demonstrated effective Rhodamine B decomposition under magnetic stirring in a dark environment, highlighting the significant influence of preparation conditions on tribocatalytic performance. Increasing the annealing temperature was observed to adversely affect the degradation rate, likely due to changes in material structure and surface area that diminish tribocatalytic activity.

Additionally, cyclic stability experiments revealed that La/ZnO samples maintained strong tribocatalytic performance over multiple cycles, indicating their robustness and reusability. The results suggest that the absorbed mechanical energy from friction effectively excites electrons and holes in the La/ZnO powders, enhancing the generation of reactive radicals responsible for dye degradation.

The study confirms that tribocatalysis offers an eco-friendly and sustainable pathway for environmental pollutant management by harnessing mechanical energy from ambient sources. This approach not only provides an alternative method for degrading organic pollutants but also aligns with green chemistry principles, presenting a promising solution for addressing environmental challenges associated with dye pollution.

Author Contributions: Conceptualization, D.K.I. and N.V.K.; methodology, N.V.K.; formal analysis, N.V.K.; investigation, D.K.I. and B.I.S.; data curation, N.V.K.; writing—original draft preparation, N.V.K.; writing—review and editing, N.V.K. and B.I.S.; visualization, D.K.I., N.V.K. and B.I.S.; supervision, N.V.K. All authors have read and agreed to the published version of the manuscript.

Data Availability Statement: Data are contained within the article.

Conflicts of Interest: The authors declare no conflicts of interest.

References

1. Jamil, T. Role of advance oxidation processes (AOPs) in textile wastewater treatment: A critical review. *Desalin. Water Treat.* **2024**, *318*, 100387. [CrossRef]
2. Ewuzie, U.; Saliu, O.; Dulta, K.; Ogunniyi, S.; Bajeh, A.; Iwuozor, K.; Ighalo, J. A review on treatment technologies for printing and dyeing wastewater (PDW). *J. Water Process. Eng.* **2022**, *50*, 103273. [CrossRef]
3. Dong, H.; Zhou, Y.; Wang, L.; Chen, L.; Zhu, M. Oxygen vacancies in piezocatalysis: A critical review. *Chem. Eng. J.* **2024**, *487*, 150480. [CrossRef]
4. Zhong, S.; Wang, Y.; Chen, Y.; Jiang, X.; Lin, M.; Lin, C.; Lin, T.; Gao, M.; Zhao, C.; Wu, X. Improved piezo-photocatalysis for aquatic multi-pollutant removal via $BiOBr/BaTiO_3$ heterojunction construction. *Chem. Eng. J.* **2024**, *488*, 151002. [CrossRef]
5. Liu, X.; Wang, T.; Li, G.; Liu, G.; Qiu, J.; Guo, Z.; Hao, H.; Dong, J.; Liu, H.; Xing, J. Cooperation or competition between piezocatalysis and photocatalysis of $Bi_4Ti_3O_{12}$ nanoflakes. *J. Alloys Compd.* **2023**, *936*, 168367. [CrossRef]
6. Kumar, M.; Kebaili, I.; Vaish, R.; El Ghoul, J.; Khandaker, M. Ball mill-induced piezocatalysis assessment for dye degradation using $BiVO_4$. *Mater. Today Commun.* **2023**, *37*, 107306. [CrossRef]
7. Djilani, C.; Zaghdoudi, R.; Djazi, F.; Bouchekima, B.; Lallam, A.; Modarressi, A.; Rogalski, M. Adsorption of dyes on activated carbon prepared from apricot stones and commercial activated carbon. *J. Taiwan Inst. Chem. Eng.* **2015**, *53*, 112–121. [CrossRef]
8. Singh, A.; Pal, D.B.; Mohammad, A.; Alhazmi, A.; Haque, S.; Yoon, T.; Srivastava, N.; Gupta, V.K. Biological remediation technologies for dyes and heavy metals in wastewater treatment: New insight. *Bioresour. Technol.* **2022**, *343*, 126154. [CrossRef] [PubMed]
9. Li, Z.; Zhang, Q.; Wang, L.; Yang, J.; Wu, Y.; He, Y. Novel application of $Ag/PbBiO_2I$ nanocomposite in piezocatalytic degradation of rhodamine B via harvesting ultrasonic vibration energy. *Ultrason. Sonochem.* **2021**, *78*, 105729. [CrossRef]
10. Tudor, M.; Borlan, R.; Maniu, D.; Astilean, S.; de la Chapelle, M.L.; Focsan, M. Plasmon-enhanced photocatalysis: New horizons in carbon dioxide reduction technologies. *Sci. Total Environ.* **2024**, *932*, 172792. [CrossRef]
11. Yang, F.; Wang, P.; Hao, J.; Qu, J.; Cai, Y.; Yang, X.; Li, C.; Hu, J. Ultrasound-assisted piezoelectric photocatalysis: An effective strategy for enhancing hydrogen evolution from water splitting. *Nano Energy* **2023**, *118*, 108993. [CrossRef]
12. Jabbar, Z.; Graimed, B.; Ammar, S.; Sabit, D.; Najim, A.; Radeef, A.; Taher, A. The latest progress in the design and application of semiconductor photocatalysis systems for degradation of environmental pollutants in wastewater: Mechanism insight and theoretical calculations. *Mater. Sci. Semicond. Process* **2024**, *173*, 108153. [CrossRef]

13. Lee, D.; Kim, M.; Danish, M.; Jo, M. State-of-the-art review on photocatalysis for efficient wastewater treatment: Attractive approach in photocatalyst design and parameters affecting the photocatalytic degradation. *Catal. Commun.* **2023**, *183*, 106764. [CrossRef]

14. Wang, J.; Hu, J.; Lu, X.; Jiang, X.; Li, J.; Liu, A.; Lu, Z.; Xie, J.; Cao, Y. Molecular scale influence mechanism of reaction raw materials on catalyst particle size and its piezoelectric catalytic performance. *Ceram. Int.* **2024**, *50*, 5285–5292. [CrossRef]

15. Yue, J.; Wu, R.; Zhang, Y.; Zhang, N.; Jing, H.; Wei, S.; Ouyang, F. The piezoelectric field-induced rearrangement of free carriers unlocks the high redox ability of $1T@_2H-MoS_2/Bi_2S_3$ piezoelectric catalyst. *Appl. Surf. Sci.* **2023**, *623*, 157033. [CrossRef]

16. Liang, Z.; Yan, C.F.; Rtimi, S.M.; Bandara, J. Piezoelectric materials for catalytic/photocatalytic removal of pollutants: Recent advances and outlook. *Appl. Catal. B Environ.* **2019**, *241*, 256–269. [CrossRef]

17. Lin, E.Z.; Kang, Z.H.; Wu, J.; Huang, R.; Qin, N.; Bao, D.H. $BaTiO_3$ nanocubes/cuboids with selectively deposited Ag nanoparticles: Efficient piezocatalytic degradation and mechanism. *Appl. Catal. B Environ.* **2021**, *285*, 119823. [CrossRef]

18. Liu, N.; Wang, R.; Gao, S.; Zhang, R.; Fan, F.; Ma, Y.; Luo, X.; Ding, D.; Wu, W. High-Performance Piezo-Electrocatalytic Sensing of Ascorbic Acid with Nanostructured Wurtzite Zinc Oxide. *Adv. Mat.* **2021**, *33*, 2105697. [CrossRef] [PubMed]

19. Ning, X.; Hao, A.; Cao, Y.; Hu, J.; Xie, J.; Jia, D. Effective promoting piezocatalytic property of zinc oxide for degradation of organic pollutants and insight into piezocatalytic mechanism. *J. Coll. Int. Sci.* **2020**, *577*, 290–299. [CrossRef]

20. Jiang, B.; Xue, X.; Mu, Z.; Zhang, H.; Li, F.; Liu, K.; Wang, W.; Zhang, Y.; Li, W.; Yang, C.; et al. Contact-Piezoelectric Bi-Catalysis of an Electrospun ZnO@PVDF Composite Membrane for Dye Decomposition. *Molecules* **2022**, *27*, 8579. [CrossRef]

21. Sharma, A.; Bhardwaja, U.; Kushwaha, H. ZnO hollow pitchfork: Coupled photo-piezocatalytic mechanism for antibiotic and pesticide elimination. *Catal. Sci. Technol.* **2022**, *12*, 812–822. [CrossRef]

22. Porwal, C.; Sharma, M.; Vaish, R.; Chauhan, V.; Ahmed, S.; Hwang, W.; Park, H.; Sung, T.; Kumar, A. Piezocatalytic dye degradation using Bi_2O_3-ZnO-B_2O_3 glass-nanocomposites. *J. Mater. Res. Technol.* **2022**, *21*, 2028–2037. [CrossRef]

23. Zhang, Q.; Jia, Y.; Chen, J.; Wang, X.; Zhang, L.; Chen, Z.; Wu, Z. Strongly enhanced piezocatalysis of $BiFeO_3$/ZnO heterostructure nanomaterials. *N. J. Chem.* **2023**, *47*, 3471–3480. [CrossRef]

24. Li, P.C.; Wu, J.; Wu, Z.; Jia, M.Y.; Ma, J.P.; Chen, W.P.; Zhang, L.H.; Yang, J.; Liu, Y.S. Strong tribocatalytic dye decomposition through utilizing triboelectric energy of barium strontium titanate nanoparticles. *Nano Energy* **2019**, *63*, 103832. [CrossRef]

25. Zhao, B.; Chen, N.; Xue, Y.; Shi, H.; Xu, H.; Li, M.; Sun, C.; Xing, Y.; Gao, B.; Ma, B. Challenges and perspectives of tribocatalysis in the treatment for dye wastewater. *J. Water Process Eng.* **2024**, *63*, 105455. [CrossRef]

26. Chong, J.; Tai, B.; Zhang, Y. Iridoparalysis effect based on ZnO with various specific surface areas for dye degradation. *Chem. Phys. Lett.* **2024**, *835*, 140998. [CrossRef]

27. Huynh, K.; Tieu, A.; Lu, C.; Smillie, L.; Nguyen, C.; Pham, S. *In-situ* engineering catalytically active surfaces for tribocatalysis with layered double hydroxide nanoparticles. *Carbon* **2024**, *228*, 119324. [CrossRef]

28. Gaur, A.; Moharana, A.; Porwal, C.; Chauhan, V.; Vaish, R. Degradation of organic dyes by utilizing $CaCu_3Ti_4O_{12}$ (CCTO) nanoparticles via tribocatalysis process. *J. Ind. Eng. Chem.* **2024**, *129*, 341–351. [CrossRef]

29. Li, X.; Tong, W.; Song, W.; Shi, J.; Zhang, Y. Performance of tribocatalysis and tribo-photocatalysis of pyrite under agitation. *J. Clean. Prod.* **2023**, *414*, 137566. [CrossRef]

30. Henniker, J. Triboelectricity in Polymers. *Nature* **1962**, *196*, 474. [CrossRef]

31. Zhao, J.; Chen, L.; Luo, W.; Li, H.; Wu, Z.; Xu, Z.; Zhang, Y.; Zhang, H.; Yuan, G.; Gao, J.; et al. Strong tribo-catalysis of zinc oxide nanorods via triboelectrically harvesting friction energy. *Ceram. Int.* **2020**, *46*, 25293–25298. [CrossRef]

32. Yang, B.; Chen, H.; Guo, X.; Wang, L.; Xu, T.; Bian, J.; Yang, Y.; Liu, Q.; Du, Y.; Lou, X. Enhanced tribocatalytic degradation using piezoelectric CdS nanowires for efficient water remediation. *J. Mater. Chem. C* **2020**, *8*, 14845–14854. [CrossRef]

33. Ruan, L.; Jia, Y.; Guan, J.; Xue, B.; Huang, S.; Wang, Z.; Fu, Y.; Wu, Z. Tribo-electro-catalytic dye degradation driven by mechanical friction using MOF-derived $NiCo_2O_4$ double-shelled nanocages. *J. Clean. Prod.* **2022**, *345*, 131060. [CrossRef]

34. Xu, Y.; Yin, R.; Zhang, Y.; Zhou, B.; Sun, P.; Dong, X. Unveiling the mechanism of frictional catalysis in water by $Bi_{12}TiO_{20}$: A charge transfer and contaminant decomposition path study. *Langmuir* **2022**, *38*, 14153–14161. [CrossRef] [PubMed]

35. Ada, K.; Gökgöz, M.; Önal, M.; Sarıkaya, Y. Preparation and characterization of a ZnO powder with the hexagonal plate particles. *Powder Technol.* **2008**, *181*, 285–291. [CrossRef]

36. Kumar, S.; Kavitha, R. Lanthanide ions doped ZnO based photocatalysts. *Sep. Purif. Technol.* **2021**, *274*, 118853. [CrossRef]

37. Tsuji, T.; Terai, Y.; Kamarudin, M.; Kawabata, M.; Fujiwara, Y. Photoluminescence properties of Sm-doped ZnO grown by sputtering-assisted metalorganic chemical vapor deposition. *J. Non Cryst. Solids* **2012**, *358*, 2443–2445. [CrossRef]

38. Khatamian, M.; Khandar, A.; Divband, B.; Haghighi, M.; Ebrahimiasl, S. Heterogeneous photocatalytic degradation of 4-nitrophenol in aqueous suspension by Ln (La^{3+}, Nd^{3+} or Sm^{3+}) doped ZnO nanoparticles. *J. Mol. Catal. A Chem.* **2012**, *365*, 120–127. [CrossRef]

39. Anandan, S.; Vinu, A.; Lovely, K.; Gokulakrishnan, N.; Srinivasu, P.; Mori, T.; Murugesan, V.; Sivamurugan, V.; Ariga, K. Photocatalytic activity of La-doped ZnO for the degradation of monocrotophos in aqueous suspension. *J. Mol. Catal. A Chem.* **2007**, *266*, 149–157. [CrossRef]

40. Duan, L.; Wang, B.; Heck, K.; Clark, C.; Wei, J.; Wang, M.; Metz, J.; Wu, G.; Tsai, A.; Guo, S.; et al. Titanium oxide improves boron nitride photocatalytic degradation of perfluorooctanoic acid. *Chem. Eng. J.* **2022**, *448*, 137735. [CrossRef]

41. Korake, P.; Dhabbe, R.; Kadam, A.; Gaikwad, Y.; Garadkar, K. Highly active lanthanum doped ZnO nanorods for photodegradation of metasystox. *J. Photochem. Photobiol. B Biol.* **2014**, *130*, 11–19. [CrossRef] [PubMed]

42. Lei, H.; Cui, X.; Jia, X.; Qi, J.; Wang, Z.; Chen, W. Enhanced Tribocatalytic Degradation of Organic Pollutants by ZnO Nanoparticles of High Crystallinity. *Nanomaterials* **2023**, *13*, 46. [CrossRef] [PubMed]
43. Sydorchuk, V.; Poddubnaya, O.I.; Tsyba, M.M.; Zakutevskyy, O.; Khyzhun, O.; Khalameida, S.; Puziy, A.M. Activated carbons with adsorbed cations as photocatalysts for pollutants degradation in aqueous medium. *Adsorption* **2019**, *25*, 267–278. [CrossRef]
44. Gan, P.P.; Li, S.F.Y. Efficient removal of Rhodamine B using a rice hull-based silica supported iron catalyst by Fenton-like process. *Chem. Eng. J.* **2013**, *229*, 351–363. [CrossRef]
45. Wu, M.; Xu, Y.; He, Q.; Sun, P.; Weng, X.; Dong, X. Tribocatalysis of homogeneous material with multi-size granular distribution for degradation of organic pollutants. *J. Colloid Int. Sci.* **2022**, *622*, 602–611. [CrossRef] [PubMed]